Nematic ordering in highly restrictive Vycor glass

G. S. Iannacchione, G. P. Crawford,* S. Qian, J. W. Doane, and D. Finotello

Department of Physics and Liquid Crystal Institute, Kent State University, Kent, Ohio 44242

S. Zumer

Department of Physics, University of Ljubljana, Jadranska 19, 61000 Ljubljana, Slovenia

Using high resolution calorimetry and deuterium nuclear magnetic resonance we report a systematic study of alkylcyanobiphenyl (nCB) liquid crystals confined to the three-dimensionally interconnected random networks of pores of Vycor glass. Composed of nearly pure SiO_2, Vycor has pores with mean diameter and chord length of ~ 70 and ~ 300 Å, respectively. We studied effects due to the severe and random confinement on the orientational order of the weak first order nematic to isotropic phase transition. For pentylcyanobiphenyl (5CB) and octylcyanobiphenyl (8CB), the nematic to isotropic (NI) transition is replaced by a continuous evolution of local microscopic orientational order extending from 15 K below to 30 K above the bulk NI transition. A modified Landau–de Gennes theory is presented to successfully model the orientational order extending from 15 K below to 30 K above the bulk NI transition. A modified Landau–de Gennes theory is presented to successfully model the orientational order within this system. From the results of the NMR analysis and with no adjustable parameters, we determine the excess heat capacity due to the orientational order and find it to be in qualitative agreement with the experiment.

PACS number(s): 64.70.Md, 61.30.−v, 65.20.+w, 82.60.Fa

I. INTRODUCTION

The confinement of physical systems to a random network of pores comprises a particularly rich area of study. Basic questions regarding how phase transitions are modified under confinement remain an issue. Experimental evidence [1–3] seem to indicate that a "random-field" model [4–7] describes the underlying physics. Phase transitions within such structures are mapped onto an Ising model developed for magnetic spin systems, with an imposed random field coupled directly to the orientational order parameter to account for the random confinement. A closely related scenario includes mapping a random uniaxial anisotropy onto a spin system [8,9] with a symmetric coupling of the anisotropy vector and the order parameter in order to account for the "up-down" symmetry of the nematic director. Recent computer simulations for this model find a specific heat peak associated with the nematic to isotropic (NI) transition shifted to lower temperatures and broadened, with no evidence of a first order nature as in bulk [10]. For sufficiently restrictive hosts, such models predict the replacement of the first order NI transition with a continuous transition to a glasslike state. The major difficulty of these models is that they do not account for the extremely slow dynamics (long relaxation times) observed for nematic fluctuations [11–13].

Recent experimental and theoretical efforts have indicated that such models may be applicable only to cases where macroscopic order is still possible, i.e., confinements which possess large interpore interactions [14–17]. However, phenomena interpreted by a random-field model may alternatively be described by phase wetting where the confinement inhibits ordered phase domain growth [18–20]. Situations where the pore structure minimizes the pore-to-pore interactions can not be expected to follow the random-field model [21–25]; an appropriate model considers interactions within a single, independent pore which are then averaged with a suitable distribution describing the confining host.

We have studied the simplest ordering that a condensed phase of matter may possess: orientational ordering in Vycor glass; a shorter version of this work has already appeared [23]. Specifically, we performed deuterium NMR (DNMR) and high resolution calorimetry measurements for liquid crystals from the alkylcyanobiphenyl (nCB, n being the number of carbons in the alkyl chain) series confined within the highly restrictive and randomly interconnected pores of Vycor glass. There is no evidence for a phase transition to a nematic phase from high temperature. Instead, there is a gradual evolution of local orientational ordering which continuously decreases with increasing temperature. These results are well explained by a "single-pore" model where the orientational ordering is dominated by intraporous interactions. Utilizing a simple expression of the Landau–de Gennes free energy density modified to include surface ordering and disordering terms, an effective scalar order parameter is calculated for a single pore. The randomness of the confinement, having a distribution of pore sizes, causes a distribution in the disordering

*Present address: Xerox, Palo Alto Research Center, Electronics and Imaging Laboratory, Palo Alto, CA 94304.

terms of the free energy. The results for a single pore are then averaged over the entire system to yield the experimentally determined response functions. The model is found to be in good agreement with both DNMR and heat capacity results.

This paper is organized as follows. A brief overview is presented in Sec. II on the experimental techniques employed and the sample preparations. Section III discusses the experimental results while Sec. III C describes the "single-pore" model and compares its predictions to experiment. We conclude by summarizing our results and discussing the implications of this approach as well as the applicability to other systems.

II. EXPERIMENTAL TECHNIQUE

Vycor "thirty" glass [26] is a porous glass made from the spinodal decomposition of a mixture of SiO_2 and BO_2. The boron oxide rich phase is etched away in an acid bath leaving a pure network of fired SiO_2 glass with a 28% porosity. The confining morphology, which is schematically represented in Fig. 1, can be described as a network of three-dimensional (3D) randomly connected pore segments with a mean pore diameter $d \sim 70$ Å, having a distribution width of ~ 5 Å, and an average length $l \sim 300$ Å [27]. The pore segments are uniformly distributed in orientation and density. The 5CB liquid crystal used exhibits in the bulk a weak first order NI transition at 308.33 K and a crystallization transition near 297 K. For 8CB, the NI transition occurs at 314.02 K followed on cooling by a smectic-A–nematic (AN) transition at 307.02 K; crystallization takes place near 295 K.

A. ac calorimetry

ac calorimetry [28] is an extremely sensitive technique that permits an accurate measurement of the heat capacity of small samples near phase transitions. The tech-
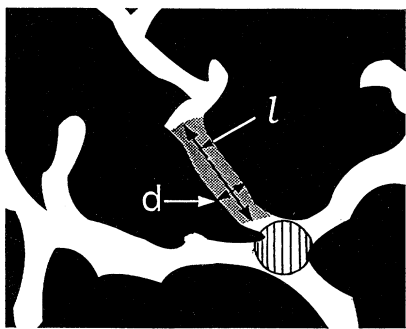
nique has been employed in precise measurements near the phase transitions of bulk [29] and confined [30] liquid crystals. Our implementation of this technique for liquid crystal research as well as to two-dimensional helium films, has already appeared in the literature [31] and only a brief review is included here.

Measurements take place under near equilibrium conditions as the sample is set into very small temperature oscillations about a precisely determined average temperature. The amplitude of the resulting temperature oscillations is inversely proportional to the heat capacity C of the sample. This amplitude T_{ac} can be written as [28,31]

$$T_{\mathrm{ac}} = \frac{Q_0}{2\omega C} \left(1 + \frac{1}{(\omega \tau_e)^2} + (\omega \tau_i)^2 \right)^{-1/2} , \qquad (1)$$

where the thermal relaxation times are defined as $\tau_e = C/K_b$ (external) and $\tau_i^2 = \tau_\theta^2 + \tau_h^2 + \tau_s^2$ (internal). The individual relaxation times are $\tau_\theta = C_\theta/K_\theta$, $\tau_h = C_h/K_h$, and $\tau_s = C_S/K_S$ corresponding to the thermometer, heater, and sample, respectively. The internal time constant is the time required for the entire assembly to reach equilibrium with the applied heat while the external time constant is the time required for equilibrium with the surrounding thermal bath.

The calorimeter has an internal time constant of approximately 1.26 s (0.79 Hz high frequency rolloff) and an external time constant of about 31.4 s (0.032 Hz low frequency rolloff). The addendum heat capacity is 42 mJ/K at 303 K and increases linearly at a rate of 0.286 mJ/K^2. The applied voltage frequency was 0.055 Hz and the induced temperature oscillations were usually 2 mK peak-to-peak. Data are taken with 10 mK steps in temperature, and after a wait of 7 min at the new temperature, it is averaged for 8 to 10 min.

The Vycor sample consisted of a small piece, 7 × 3 mm, shaved to < 0.5 mm thick. It weighed ~ 11 mg and was later filled with ~ 2.5 mg of either 5CB, 7CB, or 8CB. The glass was boiled in a 30% solution of hydrogen peroxide and distilled water bath, and ultrasonically agitated for several hours before drying under vacuum at $\sim 100\,°C$. The glass piece was then immediately placed in an isotropic bath of the desired liquid crystal for 12 h. While in the isotropic phase, the sample was wiped with Whatman absorbent filter paper to remove the excess liquid crystal.

B. Deuterium nuclear magnetic resonance

Nuclear magnetic resonance is an extremely valuable tool for the study of liquid crystals as it probes the orientational order, director configurations, and molecular dynamics and relaxation. Deuterium NMR has been successfully applied to the study of bulk [32] and, more recently, to confined [33] liquid crystals.

The spectrometer used in this study consists of a 4.7 T (200 MHz for protons, 30.8 MHz for deuterium) superconducting magnet fitted with a homemade probe and electronics. The probe head is inserted in an oven also

FIG. 1. Schematic of the pore structure of Vycor glass. Note the independent pore segments characterized by a length l and diameter d and the interconnection region (designed by the shaded circle) where several pore segments join together.

housed in the magnet bore, through which a mixture of ethylene glycol and water circulates to an external temperature controlled bath. The probe head is provided with a calibrated 100 Ω platinum thermometer which is read after each NMR pulse sequence and averaged over the accumulated scans. The temperature stability over the entire acquisition time is between than ± 0.05 K with a resolution of ± 0.005 K.

The DNMR sample consisted of a clean Vycor cylinder $\sim$ 5 mm in diameter and 15 mm long, filled with either 5CB or 8CB, both having a CD_2 group in the first position of the alkyl hydrocarbon chain (α deuterated). Measurements were performed both heating and cooling after thermally cycling the sample several times about the bulk NI transition in the NMR field.

Measurements used a quadrupole-echo pulse sequence (90°_x-τ-90°_y-τ-acquisition) with full phase cycling: $\tau \cong$ 100 μs, $90^\circ \cong 3$ μs, a 1000 to 2000 point acquisition, and a last delay of 300 ms. This sequence was accumulated for up to 50 000 scans over a two hour period. The resulting spectra, after Fourier transform of the single zero-filled free induction decay, is interpreted via the relationship [32,34]

$$\Delta\nu = \tfrac{1}{2}\Delta\nu_0 S(3\cos^2\theta_B - 1) , \qquad (2)$$

where $\Delta\nu_0$ is the maximum possible splitting observable for a given nematic, S is the scalar order parameter, and θ_B is the angle that the nematic director makes with the static NMR field.

For a typical bulk liquid crystal sample, the splitting, $\Delta\nu_{bulk} = \Delta\nu_o S_{bulk}$, is between two sharp absorption lines, typically 200–400 Hz full width at half maximum (FWHM). For a confined sample having a single scalar order parameter S (often smaller than bulk's) but a distribution of the nematic director orientation, a powder pattern is observed. For instance, for a spherical distribution of the director, shoulders with a splitting equal to $\Delta\nu_{bulk}$ and 90° singularities with a splitting $\tfrac{1}{2}\Delta\nu_{bulk}$ for the same scalar order parameter would be seen [34]. A spherical distribution represents the most isotropic distribution possible. If a distribution in the scalar order parameter not centered at $S = 0$ also exists, then, a superposition of spherical powder patterns is observed having the same distribution. The FWHM of this pattern would be $\Delta\nu = \tfrac{1}{2}\Delta\nu_0 S$. If this distribution in S is narrow and centered at $S = 0$, then, a single sharp Lorentzian absorption peak, FWHM $\sim$ 50 Hz, due to motional averaging as for isotropic bulk liquid crystals is observed.

III. RESULTS AND DISCUSSION

A. Deuterium NMR

At all temperatures for both 5CB and 8CB confined to Vycor, a single and broad absorption peak reminiscent of a bulk isotropic peak is observed. At 30 K above the bulk NI transition (T^b_{NI}), the FWHM is $\sim$ 0.8 kHz, growing continuously to $\sim$ 12 kHz when cooled to 15 K below

$T_N I^b$. From the discussion in Sec. II, an accurate measurement of the FWHM is an important quantity, therefore, line shape fits were done using various functions. A true isotropic peak is characterized by a single Lorentzian line shape, however, the spectra observed here is not completely fitted by such a single Lorentzian (see Fig. 2). The deviations suggest the existence of a sharper component and in fact, excellent fits were obtained by superimposing two Lorentzians consisting of a broad (FWHM $\sim$ 1 kHz) and a narrow (FWHM $\sim$ 0.2 kHz) component. Attempts at fitting the spectra by other combinations of Gaussian and Lorentzian line shapes proved unsatisfactory. Thus, in order to accurately determine the FWHM, all spectra were analyzed using an artificially introduced double Lorentzian and recording the individual FWHM and the percent contribution to the total area under the peak, as a function of temperature. Since the magnetic coherence length ($\sim$ 1.2 μm) [35] is much larger than the pore size, the static magnetic field has a negligible effect on the nematic order within the pores. The spectral patterns are independent of the samples orientation within the static magnetic field, confirming the random nature of the Vycor porous network.

A single broad absorption peak may be attributed to diffusion induced motional averaging over randomly ori-
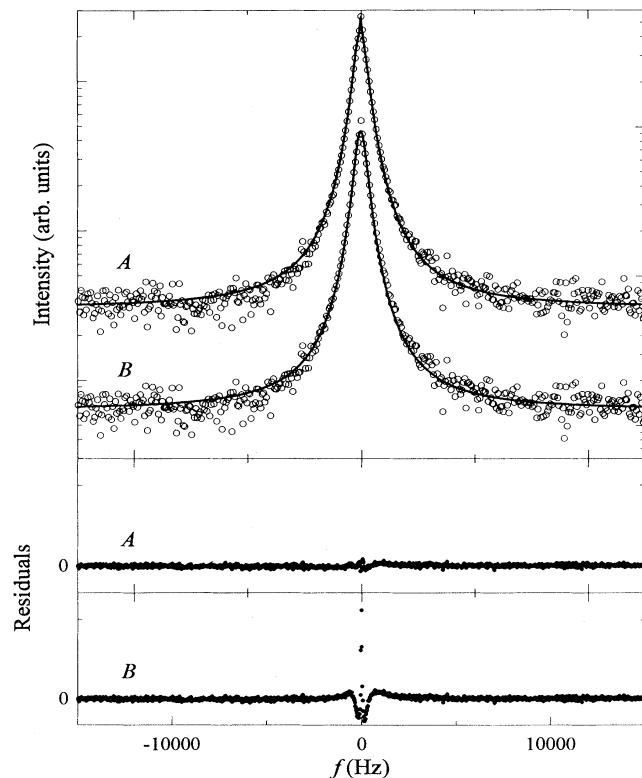

FIG. 2. Semilogarithmic plot of the DNMR absorption spectra for 5CB-αd_2 in Vycor at 55°C. Fitting with a double Lorentzian (A) yields a near perfect fit compared with a single Lorentzian that fails to fit the data near the peak maximum (B). For clarity, only every other data point is plotted. The residuals of the fits are given in the lower panels with a scale 4% of the upper intensity plot.

ented nematic domains, to a distribution of weakly ordered nematic areas, or more realistically, to some intermediate case. To determine which situation applies here, we note that the modulation of the quadrupolar coupling induced by translational self-diffusion of liquid crystal molecules among pore segments of length l is characterized by a time $\tau_0 \sim l^2/2D$, with D the effective diffusion constant. The diffusion is certainly hindered by surface interactions causing possible bonding of the molecules to the glass surface as observed in other systems [36,37]. Using a typical bulk value of 10^{-11} m^2/s for D [36,37] and $l = 300$ Å we obtain an overestimate for the diffusion induced modulation rate: $\tau_0^{-1} \approx 2 \times 10^4$ s^{-1}. A modulation at such a rate can substantially affect the spectra when the splitting $\Delta\nu < (2\pi\tau_0)^{-1}$ [34]. Here, only far above T_{NI}^b, where $\Delta\nu < 1$ kHz, is such a condition realized. There, the modulated quadrupole couplings have an amplitude $\omega_q \sim \pi\langle\Delta\nu\rangle$ and one can use $T_2^{-1} \sim \omega_q^2\tau_0$ to estimate the width of the resonance line [34]. In Vycor, such a broadening is much smaller than $\langle\Delta\nu\rangle$. Thus, to a good approximation, the DNMR spectrum reflects the static distribution from the pore segments individual contribution. The contribution is motionally averaged over the suppressed nematic order within each pore segment.

Figure 3 shows the temperature dependence of the FWHM of the broad component for 5CB and 8CB. The broad component contributes more than 90% to the total signal (area under the peak); its temperature dependence for both liquid crystals is shown in Fig. 4. The broad component is likely due to the liquid crystal confined to the 300 Å long pore segments. The narrow component cannot be due to bulk outside of the Vycor as it does not
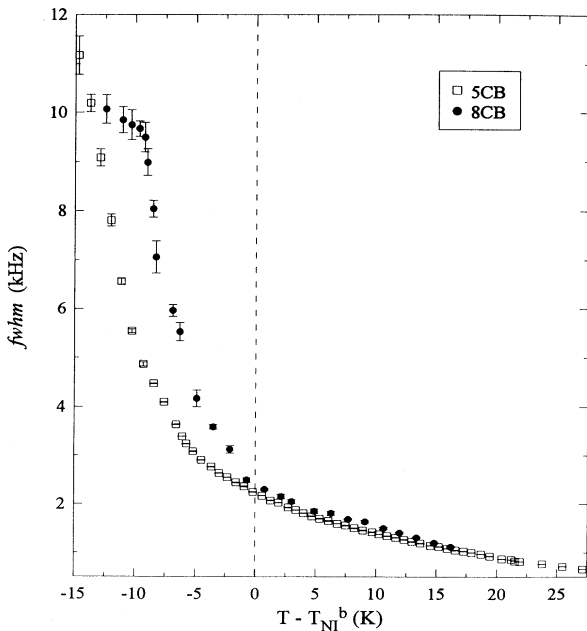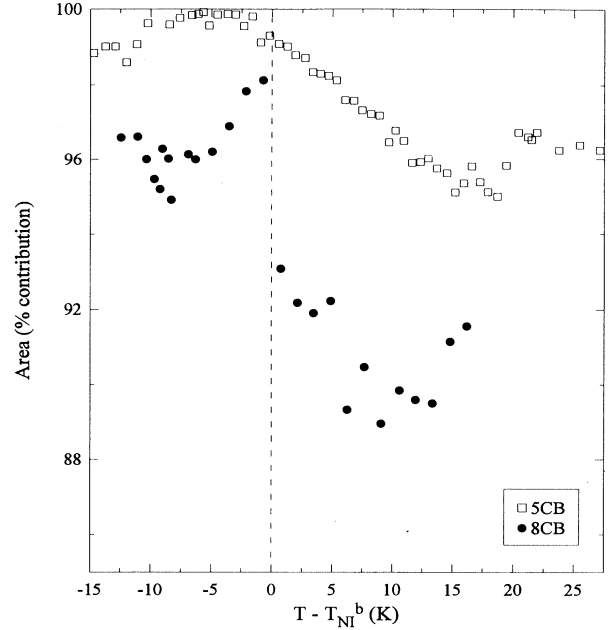

FIG. 4. Percent contribution to the total DNMR peak area of the broad component [A_B (in %)] which is proportional to the number of orientationally ordered molecules. Note the jump in contribution at T_{NI} for 8CB not seen in 5CB.

show any quadrupolar splitting at or below T_{NI}^b. Also, since at most it yields $\sim 10\%$ of the total single, such an amount of bulk would be easily visible on the outside of the Vycor cylinder. Therefore, this narrow Lorentzian component may be associated with the void regions joining pore segments. These regions, nearly spherical and ~ 70 Å in diameter, contain defects, randomly oriented directors, and a distribution of order parameters which would most likely result in a motionally averaged isotropiclike peak. The importance of pore "end effects" in these systems was recently shown by Tripathy, Rosenblatt, and Aliev [25].

The temperature dependence of the FWHM for both components is distinctly different. For the broad component it increases smoothly from ~ 0.8 kHz with decreasing temperature; it is almost identical for 8CB and 5CB near and above T_{NI}^b. Below T_{NI}^b, the FWHM for 8CB grows faster, eventually saturating at ~ 11 kHz near $\Delta T = T - T_{NI}^b \approx -10$ K. This may be an indication that smectic ordering (present in bulk 8CB) couples with the nematic and increases the rate of growth of orientational order. In contrast, the narrow component for both liquid crystals is identical and essentially temperature independent with a width of ~ 200 Hz which is still a factor of ~ 4 greater than bulk. Thus, given the percent contribution and the temperature dependence, the broad component essentially contains the physics of this system.

The percent contribution to the total area of the absorption peak from the broad component [A_B (%)] shows interesting differences between 5CB and 8CB. The temperature dependence of the narrow component is, of

FIG. 3. The FWHM of the broad (orientationally ordered) component for 5CB (□) and 8CB (•) confined to Vycor.

course, $100\%-[A_B \, (\%)]$. As seen in Fig. 4, the $[A_B$ (%)] for 8CB is lower than that for 5CB at all temperatures. Both liquid crystals show $[A_B \, (\%)]$ increasing with decreasing temperature but 8CB also exhibits a sudden jump near T_{NI}^b while that of 5CB monotonically grows until reaching a maximum near $\Delta T \approx -5$ K. Below the 5CB maximum and below the jump in 8CB, $[A_B \, (\%)]$ gradually decreases. The sudden jump in $[A_B \, (\%)]$ in 8CB may be due to subtle smectic influences while the gradual decrease in $[A_B \, (\%)]$ below the maximum indicates a slow freezing out of the molecular motions with spin-spin relaxations becoming progressively shorter than the delay used in the quadrupole-echo pulse sequence. The single absorption peak becomes unobservable for both 5CB and 8CB below $\Delta T \approx -15$ K. The area under the absorption peak is sensitive to the repetition rate of the quadrupolar-echo sequence, which, if comparable to the spin-lattice relaxation time (T_1) can saturate the spectra. The T_1 of the confined sample was found to be ~ 10 ms using an inversion-recovery sequence [34] which is ~ 30 times less than the last delay; confinement and lowering temperatures are expected to further decrease
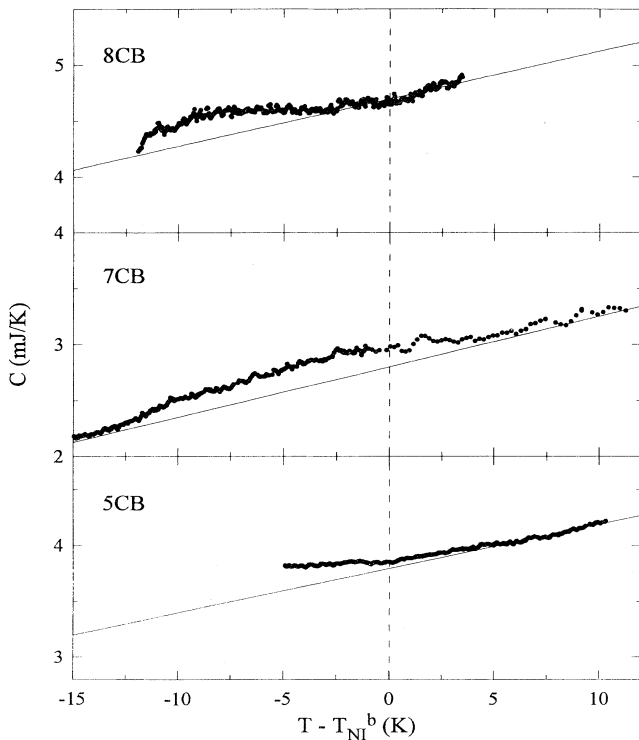

FIG. 5. Heat capacity of 5CB, 7CB, and 8CB (after subtracting the Vycor glass contribution) plotting against $T - T_{NI}^b$. The highest temperature heat capacity exhibits the same temperature dependence for all liquid crystals. A broad and suppressed "bump" is clearly seen when this high temperature behavior (indicated by the solid line) is extrapolated to lower temperatures.

T_1 [38]. Thus T_1 saturation is not expected to seriously affect the area under the absorption peaks.

B. Calorimetry

The DNMR measurements find no evidence of a typical NI transition, i.e., the spectral pattern does not evolve from a single absorption peak (isotropic phase) into a quadrupolar splitting (nematic phase). This suggests that no heat capacity signature should be present. Indeed, results from high resolution ac calorimetry found no evidence for any NI transition for 5CB, 7CB, or 8CB confined to Vycor glass. The heat capacity as a function of temperature, after subtraction of the glass contribution, is shown in Fig. 5. At temperatures above T_{NI}^b, and for all nCB studied, a linear heat capacity behavior with a stronger than bulk temperature dependence (a slope of 0.041 mJ/K^2) is observed; it deviates from linearity only in the vicinity of the bulk transition T_{NI}^b. By extrapolating this linear high temperature background to lower temperatures and subtracting it from the data, a broad and rounded "bump" emerges. This is consistent with differential scanning calorimetry results that have also shown the existence of a similar "bump" for 8CB confined to Vycor [24] and p-azoxyanisole (PAA) confined to various controlled porous glasses (CPGs) [39]. It is attributed to the development of local orientational order within the system. Due to the uncertainties in the small mass of the samples ($\sim 20\%$), no specific heats were calculated as a comparison with bulk values would not be reliable.

C. Local orientational order: "single-pore" model

To estimate the influence of the local structure of the pore segment or the interaction between neighboring pores on the orientational order, the ratio of the surface of the glass-liquid crystal interface within a pore segment (l) to the surface at the ends of the segments (d) is determined. See Fig. 1. The ratio $l/d \approx 4$ suggests that the porous network may be approximated by a collection of weakly interacting pore segments where the order is primarily determined by local (intraporous) constraints. Collective (interporous) interactions can thus be ignored.

The behavior of a liquid crystal phase in each independent pore segment may be explained using a simplified Landau approach. Given the 35 Å pore radius, at least 50% of the molecules are in contact with the surface. Neglecting details like biaxiality, the liquid crystal orientational order in a pore can be described by an average molecular orientation along the pore and an effective scalar order parameter S [35] obtained by averaging over a pore. In a free energy expansion

$$f = f_0 + \tfrac{1}{2}a(T - T^*)S^2 - \tfrac{1}{3}bS^3 + \tfrac{1}{4}cS^4 + hS^2 - gS \, ,$$

$$(3)$$

with f_0, a, T^*, b, and c being measured phenomenological

Landau parameters [35,40]; the hS^2 and $-gS$ terms are added to describe the confinement induced constraints. This is similar to what has been done in less restrictive geometries to describe surface effects [40,41]. Minimization of the above free energy yields the temperature dependence of the order parameter S.

The hS^2 term describes the disordering effects of surface induced deformations. As these strongly depend on the pore shape and the roughness of its surface, h is expected to vary from pore to pore. Introducing R as the effective radius of curvature of the surface, it is estimated that $h \sim L/R^2$, where L represents the Landau-de Gennes expansion coefficient characterizing all terms having second order derivatives of the order parameter [40,42]. The $-gS$ term describes the ordering effect of the surface interaction; g is thus expected to be independent of the detailed shape, but proportional to the surface to volume ratio. The magnitude of g is estimated by $g = 4W/d$ where W is the surface anchoring strength of the liquid crystal on a SiO_2 glass surface and d is the diameter of the pore.

The standard part of the free energy, the first four terms in Eq. (3), describes the bulk first order NI phase transition at $T_{NI}^b = T^* + 2b^2/9ac$; inclusion of the hS^2 disordering term depresses the transition temperature by an amount $\Delta T = 2h/a = 2L/(aR^2)$. The effect of h may thus be viewed as a renormalization of T^*. Using typical values for L and a [40,42], and the average pore radius as an estimate for R, the NI transition is expected to shift downward by ~ 30 K. The effect of $-gS$ is analogous to that of an external magnetic field on a spin system, and replaces a discrete phase transition by a continuous evolution of order which becomes more gradual with increasing g. Under less severe constraints (pore larger than the nematic correlation length), where surface effects are limited to the boundary layer and not describable by our simplified model, the NI transition is only shifted by 1 to 3 K [14,15,17,30,42,42,43].

Due to the pores relatively elongated shape, the local director within a pore should not deviate considerably from the average one. According to our approximation, the system can be represented by a Gaussian distribution $w(h)$ in the disordering parameter arising from a distribution in the pore's effective curvature. The distribution is characterized by an average disordering parameter h_0 and width σ. These enable a calculation of the expected response functions of the total system by averaging individual contributions over $w(h)$ (process denoted by $\langle\ \rangle$). Further, we also neglect possible correlations between the order parameter S and the angle θ_B which is taken to be randomly distributed. Each h produces an individual powder pattern [34], and the observed DNMR spectrum is the superposition of such patterns arising from a distribution of h. The FWHM $\langle\Delta\nu\rangle$ of the resulting broad component of the single peak spectrum is approximately given by $\frac{1}{2}\Delta\nu_0\langle S\rangle$.

A simulation based on the superposition of spherical powder patterns with a Gaussian distribution in the scalar order parameter is shown in Fig. 6. The simulation shows a nearly Lorentzian line shape with a small feature at the peak maximum. This splitting is due to the

center of the order parameter distribution being greater than zero which could dominate the final average. A plot of the FWHM (scaled by the bulk coupling constant ν_0) against the average scalar order parameter (inset of Fig. 6) exhibits a linear dependence with zero intercept.

To explore the effect of the surface terms in our model, $\langle S\rangle$ is calculated as a function of three crucial variables: center of the effective curvature distribution, width of this distribution, and the surface ordering coupling constant, and is compared to the DNMR result of 5CB. Using bulk 5CB parameters (a, T^*, b, c, L) [36,44], the average scalar order parameter is calculated for various $2h_0/a$, $2\sigma/a$, and g. For each varied parameter, the other two were fixed at values close to those that better matched the experimental results. As expected, varying h_0 simply shifts $\langle S\rangle$ in temperature while varying σ adjusts the curvature of the temperature dependence of $\langle S\rangle$. Varying g mainly shifts the absolute magnitude of $\langle S\rangle$ at all temperatures. The effect of the variations of these parameters is evident from Fig. 7.

With bulk parameters for 5CB and 8CB and the above calculations as a starting point, a good fit of the temperature dependence of $\langle S\rangle$ is obtained as seen in Fig. 8. The resulting parameters for $2h_0/a$, $2\sigma/a$, and g for 5CB and 8CB are given in the inset. Expressing $2h_0/a$ in terms
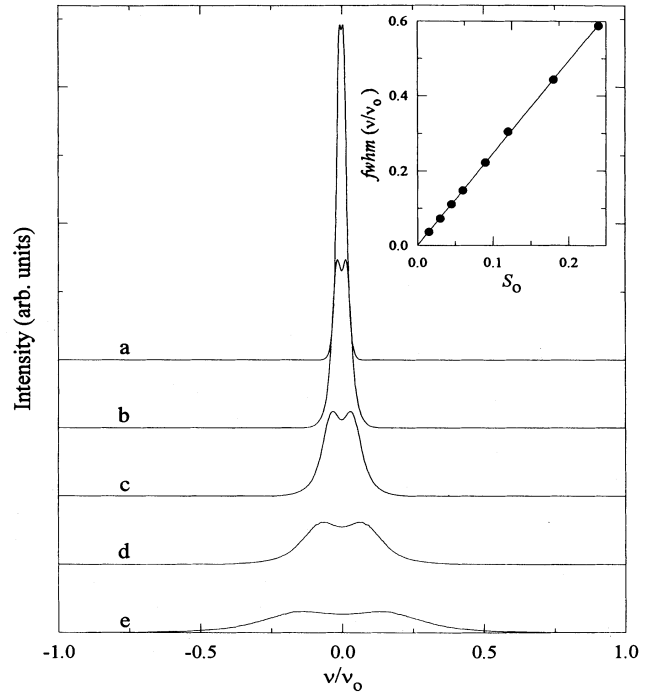

FIG. 6. DNMR line shape simulation based on a superposition of spherical powder patterns having a Gaussian distribution in the scalar order parameter S. The simulations labeled a–e have S_0 (a scaling factor shifting the center of the distribution) progressively doubled. Inset: the normalized FWHM of the simulated line shape versus S_0 showing its linear behavior.

of an effective surface radius of curvature, the results for both 5CB and 8CB yield a consistent $\langle R \rangle = (L/h_0)^{1/2} = 35 \pm 0.5$ Å, which is identical to the average pore radius for Vycor [27]. In addition, converting the width of the disordering distribution to the corresponding width in the pore size distribution, $\Delta R = R(h_0 + \sigma) - R(h_0 - \sigma)$, for both 5CB and 8CB one finds 7 ± 0.5 Å which is consistent with the width of the pore size distribution for Vycor [27]. The surface coupling constant (g) is larger than that for bare glass and larger for 8CB than 5CB. This is not surprising since acid treated SiO_2 glass generally has a stronger surface anchoring energy [45] and the surface anchoring strength usually increases with chain length of a liquid crystal homolog [46].

An attempt to fit a normalized amplitude and frequency spectra of 5CB in Vycor at 29.98°C based on our model was carried out. Given the behavior of the model presented in Fig. 6, a narrow Lorentzian with a width fixed at 180 Hz is added to account for the sharply peaked nature of the measured spectra. By adjusting the width and center of the distribution in h and a multiplica-

tive factor controlling the order parameter Q_0, a reasonable match to the experimental spectra was obtained, see Fig. 9. The simulated spectra strongly resembles the broad and narrow Lorentzian (see inset of Fig. 9) used in the analysis of the experimental spectra. The resulting parameter $2h_0/a = 21$ K is identical but $2\sigma/a = 7$ K is larger than those found by fitting the temperature dependence of $\langle S \rangle$. The differences in the width may be due to neglecting motional averaging and line broadening [34] which would lower the required width σ for a good match.

The heat capacity of a liquid crystal in a porous network of volume V described by the "single-pore" model is obtained from the mean-field relation, $\langle \Delta C \rangle = \frac{1}{2} aVT |\partial \langle S \rangle^2/\partial T|$ [47]. This calculation yields a very suppressed bump centered at approximately $T_{NI}^b - 2h_0/a$ and broadened on the order of g/a. The model predicted $\langle \Delta C \rangle$ is calculated with the appropriate bulk and fit parameters for 5CB, 7CB, and 8CB, resulting in a predicted bump centered approximately 15–20 K below the bulk NI transition [23]. Although large in size, they are mostly a consequence of the simplicity the model employed. The fit parameters for 7CB were estimated from the DNMR fit results of 5CB and 8CB (no DNMR stud-
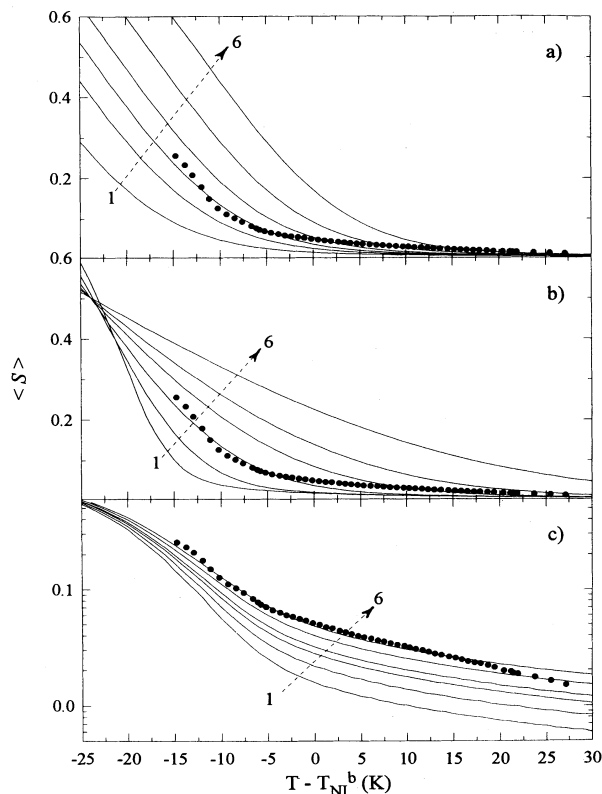

FIG. 7. Six model calculated $\langle S \rangle$ (solid lines) overlaid by the experimental results for 5CB (•); (a) $2h_0/a$ varies in order as 4, 10, 15, 19, 25, and 30 K, respectively, with $2\sigma/a = 10$ K and $g = 1 \times 10^5$ J/m^3; (b) $2\sigma/a$ varies in order as 3, 6, 10, 15, 20, 30 K, respectively, with $2h_0/a = 22$ K and $g = 1 \times 10^5$ J/m^3; and (c) g varies in order as 7, 8, 9, 10, 11, 12 $\times 10^4$ J/m^3, respectively, with $2h_0/a = 22$ K and $2\sigma/a = 4$ K.
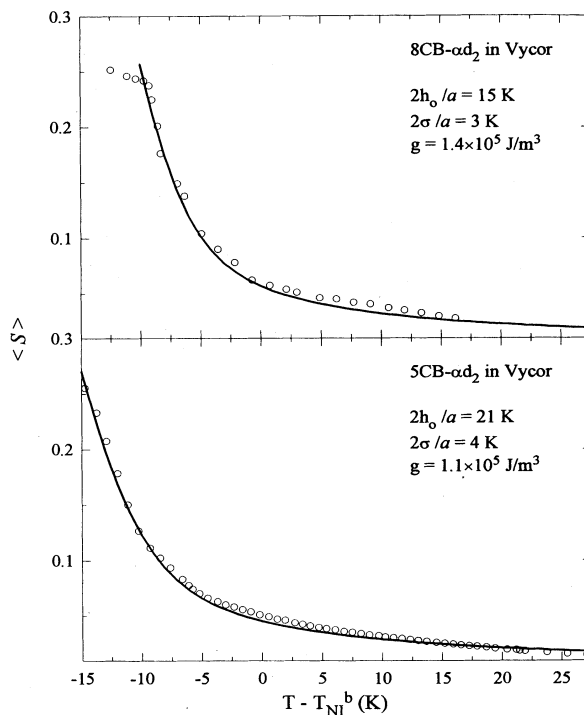

FIG. 8. Best fit to $\langle S \rangle$ for 8CB (top) using $2h_0/a = 15$ K, $2\sigma/a = 3$ K, and $g = 1.4 \times 10^5$ J/m^3, and of 5CB (bottom) using $2h_0/a = 21$ K, $2\sigma/a = 4$ K, and $g = 1.1 \times 10^5$ J/m^3. Using the appropriate Landau expansion coefficient a for each liquid crystal, a consistent mean pore radius of $R = 35 \pm 0.5$ Å and width of the pore size distribution of 7 ± 0.5 Å, nearly identical to that determined experimentally by nitrogen isotherms [26] are found.

ies for 7CB in Vycor are available). Figure 10 shows the experimental heat capacity ΔC_p, after subtraction of the linear background not associated with the local orientational ordering and the calculated $\langle \Delta C \rangle$. Unfortunately, our experiments with 5CB in Vycor were limited to the vicinity of room temperature where the deviation from the linear background is only beginning to become apparent. For all liquid crystals, the initial rise and magnitude of the heat capacity on cooling are in qualitative agreement with the model predictions using h_0, σ, and g as determined by DNMR, without any additional fitting parameters. Under the same constraints, the 7CB and 8CB samples, of higher T_{NI}^b than 5CB, clearly show the model-predicted bump. However, the model locates the bump at lower temperatures and with a maximum order of magnitude greater than what is observed by both ac and differential scanning (DS) calorimetry [24]. This discrepancy is likely due to the simplified model also neglecting end effects [25], and considering only the slow freezing of local orientational order, thus ignoring the glasslike freezing of the mobility of the LC molecules.

Despite the large uncertainty in the sample's mass, the transition enthalpy (ac calorimetry is not sensitive to latent heats l_{NI}), the integral of ΔC per unit mass ($\delta H = \int \Delta C_p dT$), is estimated to be 0.13 ± 0.03, 0.8 ± 0.2, and

FIG. 10. Excess heat capacity associated with the orientational ordering for 5CB, 7CB, and 8CB together with the model predicted heat capacities. The model reproduces the magnitude of the heat capacity above the "bump" and the initial curvature, however, the model predicts a "bump" maximum and shifted position too large compared to the experiment. This is perhaps due to the model neglecting effects like slow, glasslike, motional freezing which are most certainly taking place.
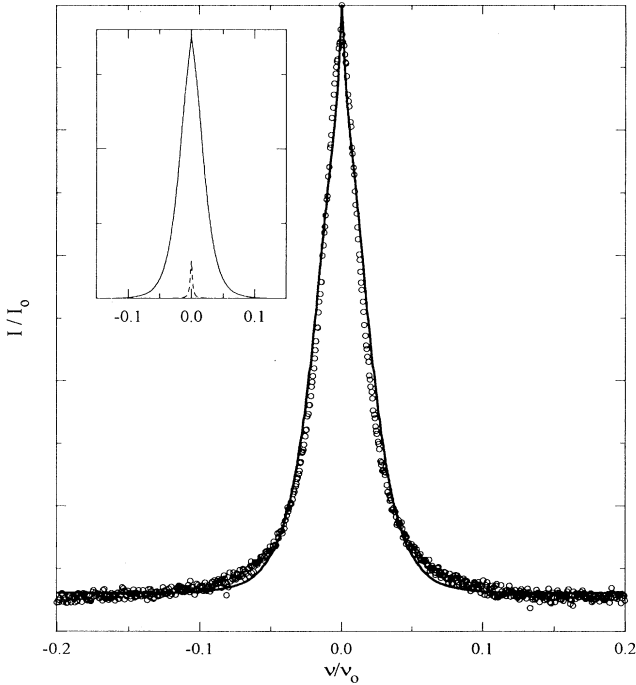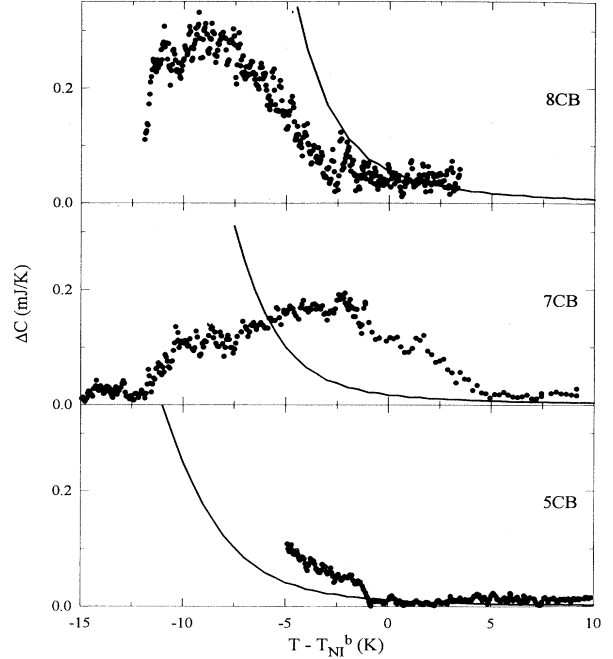

FIG. 9. Comparison of a normalized intensity and frequency spectra of 5CB in Vycor ($\circ$) at 29.98 °C to the independent-pore model with the addition of a narrow Lorentzian (solid line). For clarity, only every other data point is plotted. Inset: the separate contributions of the original model (solid line) and narrow Lorentzian (dashed line), the original model accounts for 98% of the total spectra.

0.7 ± 0.2 J/g for 5CB, 7CB, and 8CB, respectively. This compares well for 7CB with its bulk value of $\delta H = 1.33$ J/g [30] and latent heat of $l_{NI} = 2.08$ J/g [48]. For 5CB, given the limited temperature range probed, would be clearly larger if the data extended to lower temperatures. Comparing to the bulk 5CB values of $\delta H = 1.16$ J/g [30] and $l_{NI} = 1.56$ J/g [48], our estimate shows that we are far from the bump maximum. For bulk 8CB, $\delta H = 2.13$ J/g [30] and $l_{NI} = 2.1$ J/g [48], compared to the 0.7 J/g for the confined case again reflects the narrow range of the observed bump which may be related to the bulk's narrow nematic range. It should be noted that ΔC_p at the NI transition can vary significantly between different batches of LC material [17]. Nevertheless, this "same order of magnitude" results lends support that the NI transition is replaced by a continuous evolution of local orientational order.

The suppressed and broad bump in Vycor, in contrast to the pronounced and less shifted peak found at the NI transition in the 175 Å pores of Aerogel [14–17], can be explained given the smaller pore size and narrower pore size distribution of Vycor. Increasing the pore size in our model by a factor of 3 changes h_0 by an order of magnitude, which may roughly describe the lesser temperature shift and peak suppression in Aerogel. Yet, it should be noted that the applicability of our model, based on an

effective order parameter, is for pore sizes as in Aerogel more qualitative than in Vycor. The different behavior of liquid crystals in Vycor as compared to Aerogel is probably not surprising since considerable differences were also found in studies of superfluid helium confined to these porous glasses [49].

IV. CONCLUSIONS

DNMR and calorimetric studies on nematic liquid crystals confined to a polymericlike network of pores show that the NI transition is replaced by a gradual increase of the local orientational order with decreasing temperature. Evidence for a frozen "isotropiclike" component is found, that most likely arises from material at the pore junctures. This is the result of the severe constraints imposed by the porous network on the liquid crystal material. A simplified model of independent subsystems (liquid crystals in pore segments) where the orientational order is described by an effective scalar order parameter, is used to describe the orientational ordering in the vicinity of the bulk NI transition. Inclusion of surface ordering and disordering terms in the Landau free energy leads to a consistent description of the DNMR and calorimetric data. Comparison of the structures of Vycor and Aerogel indicates that in the latter case the interporous interaction should be stronger. There, a model including intraporous and interporous interactions must be used.

To establish which collective effects should be expected in random systems, it is useful to stress the distinctions and similarities with magnetic systems. Excluding polar effects, liquid crystal molecules do not distinguish between "up" and "down." Thus, the intraporous (surface induced) orientational ordering mechanism resembles more the "random uniaxial anisotropies" than the "random fields" in the Heisenberg spin models [8,9]. The randomness of preferred molecular orientations in different parts of the porous network is glasslike, but, unlike spin systems [4–7], the "up-down" symmetry prevents the system from undergoing a glass to disordered state transition. Order is expected to continuously decrease with increasing temperature as in the spin system with random fields [6]. Since elastic constants are proportional to S^2, the slowing down of long wavelength fluctuations in such systems should be caused by the decreasing interporous coupling with temperature rather than by the critical slowing down associated with the orientational glass-isotropic transition.

[1] M. C. Goh, W. I. Goldberg, and C. M. Knobler, Phys. Rev. Lett. **58**, 1008 (1987).

[2] S. B. Dierker and P. Wiltzius, Phys. Rev. Lett. **58**, 1865 (1987); Phys. Rev. Lett. **66**, 1185 (1991).

[3] P. Wiltzius, S. B. Dierker, and B. S. Dennis, Phys. Rev. Lett. **62**, 804 (1989); S. B. Dierker, B. S. Dennis, and P. Wiltzius, J. Chem. Phys. **92**, 1320 (1992).

[4] F. Brochard and P. G. de Gennes, J. Phys. Lett. (Paris) **44**, 785 (1983).

[5] P. G. de Gennes, J. Phys. Chem. **88**, 6469 (1984).

[6] K. Binder and A. P. Young, Rev. Mod. Phys. **58**, 801 (1986) and references therein.

[7] A. Maritan, M. Cieplak, T. Bellini, and J. R. Banavar, Phys. Rev. Lett. **72**, 4113 (1994); A. Maritan, M. Cieplak, and J. R. Banavar, in *Liquid Crystals in Complex Geometries Formed by Polymer and Porous Networks*, edited by G. P. Crawford and S. Zumer (Taylor and Francis, London, in press).

[8] Y. Y. Goldschmidt and A. Aharony, Phys. Rev. B **32**, 264 (1985).

[9] K. Uzelac, A. Hasmy, and R. Jullien, Phys. Rev. Lett. **74**, 422 (1995).

[10] D. J. Cleaver, S. Kralj, T. J. Sluckin, and M. P. Allen, in *Liquid Crystals in Complex Geometries Formed by Polymer and Porous Networks*, edited by G. P. Crawford and S. Zumer (Taylor and Francis, London, in press).

[11] X-l. Wu, W. I. Goldberg, M. X. Liu, and J. Z. Xue, Phys. Rev. Lett. **69**, 470 (1992).

[12] F. Aliev, W. I. Goldberg, and X-l. Wu, Phys. Rev. E **47**, R3834 (1993).

[13] M. Y. Lin, S. K. Sinha, J. M. Drake, X-l. Wu, P. Thiyagarajan, and H. B. Stanley, Phys. Rev. Lett. **72**, 2207 (1994); G. Schwalb and F. W. Deeg, *ibid.* **74**, 1383 (1995).

[14] T. Bellini, N. A. Clark, C. D. Muzny, L. Wu, C. W. Garland, D. W. Schaefer, and B. J. Oliver, Phys. Rev. Lett. **69**, 788 (1992)

[15] N. A. Clark, T. Bellini, R. M. Malzbender, B. N. Thomas, A. G. Rappaport, C. D. Muzny, D. W. Schaefer, and L. Hrubesh, Phys. Rev. Lett. **71**, 3505 (1993).

[16] T. Bellini, N. A. Clark, and D. W. Schaefer, Phys. Rev. Lett. **74**, 2740 (1995).

[17] L. Wu, B. Zhou, C. W. Garland, T. Bellini, and D. W. Schaefer, Phys. Rev. E **51**, 2157 (1995).

[18] A. J. Liu, D. J. Durian, E. Herbolzheimer, and S. A. Safran, Phys. Rev. Lett. **65**, 1897 (1990).

[19] A. J. Liu and G. S. Gest, Phys. Rev. A **44**, R7894 (1991).

[20] L. Monette, A. J. Liu, and G. S. Gest, Phys. Rev. A **46**, 7664 (1992).

[21] F. M. Aliev and M. N. Breganov, Zh. Eksp. Teor. Fiz. **95**, 122 (1989) [Sov. Phys. JETP **68**, 70 (1989)]; F. M. Aliev and K. S. Pozhivilko, Pis'ma Zh. Eksp. Teor. Fiz. **49**, 271 (1989) [JETP Lett. **49**, 308 (1989)].

[22] S. Kralj, G. Lahajnar, A. Zidansek, N. Vrbancic-Kopac, M. Vilfan, R. Blinc, and M. Kosec, Phys. Rev. E **48**, 340 (1993).

[23] G. S. Iannacchione, G. P. Crawford, S. Zumer, J. W.

Doane, and D. Finotello, Phys. Rev. Lett. **71**, 2595 (1993).

[24] G. S. Iannacchione, S. Qian, G. P. Crawford, S. S. Keast, M. E. Neubert, J. W. Doane, D. Finotello, L. M. Steele, P. E. Sokol, and S. Zumer, Mol. Cryst. Liq. Cryst. **262**, 13 (1995).

[25] S. Tripathi, C. Rosenblatt, and F. M. Aliev, Phys. Rev. Lett. **72**, 2725 (1994).

[26] Corning, Inc., Corning, NY 14831.

[27] P. Levitz, G. Ehret, S. K. Sinha, and J. M. Drake, J. Chem. Phys. **95**, 6151 (1991).

[28] P. Sullivan and G. Seidel, Phys. Rev. **173**, 679 (1969).

[29] C. W. Garland, in *Phase Transitions in Liquid Crystals*, edited by S. Martellucci and A. N. Chester (Plenum, New York, 1992) and references therein.

[30] G. S. Iannacchione and D. Finotello, Phys. Rev. Lett. **69**, 2094 (1992); Phys. Rev. E **50**, 4780 (1994).

[31] L. M. Steele, G. S. Iannacchione, and D. Finotello, Rev. Mex. Fis. **39**, 588 (1993).

[32] J. W. Doane, in *Magnetic Resonance of the Phase Transitions*, edited by F. J. Owens, C. P. Poole, and H. A. Farach (Academic, New York, 1979).

[33] G. P. Crawford, R. Stannarius, and J. W. Doane, Phys. Rev. A **44**, 2558 (1991); D. W. Allender, G. P. Crawford, and J. W. Doane, Phys. Rev. Lett. **67**, 1442 (1991); R. J. Ondris-Crawford, G. P. Crawford, S. Zumer, and J. W. Doane, Phys. Rev. Lett. **70**, 194 (1993).

[34] A. Abragam, *The Principles of Nuclear Magnetism* (Clarendon, Oxford, 1962).

[35] P. G. de Gennes, *The Physics of Liquid Crystals* (Clarendon, Oxford, 1974).

[36] G. P. Crawford, D. K. Yang, S. Zumer, D. Finotello, and J. W. Doane, Phys. Rev. Lett. **66**, 72 (1991); G. P. Crawford, R. J. Ondris-Crawford, S. Zumer, and J. W.

Doane, *ibid.* **70**, 1838 (1993).

[37] M. Vilfan, V. Rutar, S. Zumer, G. Lahajnar, R. Blinc, J. W. Doane, and A. Golemme, J. Chem. Phys. **89**, 597 (1988).

[38] N. Vrbancic, M. Vilfan, R. Blinc, J. Dolinsek, G. P. Crawford, and J. W. Doane, J. Chem. Phys. **98**, 3540 (1993).

[39] M. D. Dadmun and M. Muthukumar, J. Chem. Phys. **98**, 4850 (1993).

[40] P. Sheng, Phys. Rev. A **26**, 1610 (1982); Phys. Rev. Lett. **37**, 1059 (1976).

[41] A. Poniewerski and T. J. Sluckin, in *Fluid Interfacial Phenomena*, edited by C. Croxton (Wiley, New York, 1986).

[42] S. Kralj, S. Zumer, and D. W. Allender, Phys. Rev. A **43**, 2943 (1991).

[43] A. Golemme, S. Zumer, D. W. Allender, and J. W. Doane, Phys. Rev. Lett. **61**, 2937 (1988).

[44] H. J. Coles, Mol. Cryst. Liq. Cryst. Lett. **49**, 67 (1978).

[45] J. Cognard, Mol. Cryst. Liq. Cryst. Supp. 1, 1 (1982); Mol. Cryst. Liq. Cryst. **64**, 331 (1981).

[46] W. Chen, L. J. Martinez-Miranda, H. Hsiung, and Y. R. Shen, Phys. Rev. Lett. **62**, 1860 (1989).

[47] M. Anisimov, V. Mammitskii, and E. Sorkin, J. Eng. Phys. (USSR) **39**, 1385 (1981); M. A. Anisimov, Mol. Cryst. Liq. Cryst. **162A**, 1 (1988).

[48] J. Thoen, in *Phase Transitions in Liquid Crystals*, edited by S. Martellucci and A. N. Chester (Plenum, New York, 1992).

[49] D. Finotello, K. A. Gillis, A. Wong, and M. H. W. Chan, Phys. Rev. Lett. **61**, 1954 (1988); M. H. W. Chan, K. I. Blum, S. Q. Murphy, G. K. S. Wong, and J. D. Reppy, *ibid.* **61**, 1950 (1988); N. Mulders, R. Mehrotra, L. S. Goldner, and G. Ahlers, *ibid.* **67**, 695 (1991).
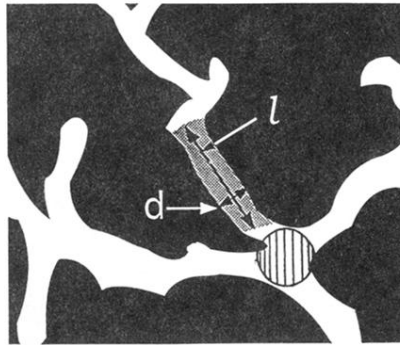
FIG. 1. Schematic of the pore structure of Vycor glass. Note the independent pore segments characterized by a length l and diameter d and the interconnection region (designed by the shaded circle) where several pore segments join together.